CHEMISTRY OF MATERIALS
Article

Chem. Mater. **2011,** *23,* 1009–1016 1009
DOI:10.1021/cm1028244

Structure, Magnetism, and Superconductivity of the Layered Iron Arsenides $Sr_{1-x}Na_xFe_2As_2$

Raquel Cortes-Gil and Simon J. Clarke*

Inorganic Chemistry Laboratory, Department of Chemistry, University of Oxford, South Parks Road, Oxford, OX1 3QR, United Kingdom

Received September 30, 2010. Revised Manuscript Received December 17, 2010

The synthesis and evolution of the structure, magnetic ordering, and superconductivity of the layered iron arsenides $Sr_{1-x}Na_xFe_2As_2$ is reported. In the $Sr_{1-x}Na_xFe_2As_2$ solid solution, the limiting Na-rich composition in samples made using conventional solid state synthesis at elevated temperatures occurs at an unusually small value ($x = 0.4$) compared with other alkali-metal-doped alkaline earth iron arsenides. Above this limiting value of the sodium content, competing phases are formed: for $x = 0.42$, an elemental iron impurity is evident, and additional impurities appear for $x > 0.42$. Superconductivity is detected in the compositions approaching the phase limit ($T_c = 26$ K for $x = 0.4$) in line with analogous isoelectronic materials. However, the magnetically ordered state which competes with the superconducting state appears not to be completely suppressed even at the limiting composition. The Na doping of $SrFe_2As_2$ is contrasted with the K-doping of $SrFe_2As_2$ and Na-doping of $BaFe_2As_2$ and other "122" iron arsenide compounds.

Introduction

The discovery of superconductivity with a high critical temperature (T_c) of 26 K in the ZrCuSiAs-type $LaFeAsO_{1-x}F_x$[1] was surprising because iron is considered antithetical to conventional *s*-wave superconductivity due to its strong magnetic moment. A large number of superconductors with FeAs antifluorite-type layers have since been discovered. These include other oxyarsenides derived from LnFeAsO with Ln = La−Dy,[2−7] and some oxyarsenides with thicker oxide layers separating the FeAs layers also exhibit superconductivity, notably Sr_2VO_3FeAs with $T_c \sim 37$ K.[8] Most investigations of these materials have focused on nonoxide ternary iron arsenides because these are more readily made phase pure and grown as large crystals than the oxide-containing materials. Many investigations have been carried out on derivatives of $BaFe_2As_2$ and $SrFe_2As_2$ ("122" materials),[9−11] and the very air-sensitive "111" materials based on LiFeAs[12−15] and NaFeAs[16,17] are now receiving more attention. Clearly, the presence of iron in layers of edge-shared $FeAs_4$ tetrahedra is a special structural motif that leads to superconductivity at unusually high temperatures, providing the electron count and structural variables are optimized. The "parent" materials with formally divalent iron such as LaFeAsO and $BaFe_2As_2$ are characterized as semimetals with Fe-3*d*-based bands crossing the Fermi surface to give hole and electron pockets. In these undoped materials, the ground state is an itinerant antiferromagnet with the magnetic ordering and an accompanying structural distortion driven by Fermi-surface nesting (i.e., spin density wave

*To whom correspondence should be addressed. E-mail: simon.clarke@chem.ox.ac.uk. Fax: +44 1865 272690. Tel: +44 1865 272600.

(1) Kamihara, Y.; Watanabe, T.; Hirano, M.; Hosono, H. *J. Am. Chem. Soc.* **2008**, *130*, 3296.
(2) Chen, X. H.; Wu, T.; Wu, G.; Liu, R. H.; Chen, H.; Fang, D. F. *Nature* **2008**, *453*, 761.
(3) Ren, Z. A.; Lu, W; Yang, J.; Yi, W.; Shen, X. L.; Li, Z. C.; Che, G. C.; Dong, X. L.; Sun, L. L.; Zhou, F.; Zhao, Z. X. *Chin. Phys. Lett.* **2008**, *25*, 2215.
(4) Chen, G. F.; Li, Z.; Wu, D.; Li, G.; Hu, W. Z.; Dong, J.; Zheng, P.; Luo, J. L.; Wang, N. L. *Phys. Rev. Lett.* **2008**, *100*, 247002.
(5) Ren, Z. A.; Yang, J.; Lu, W.; Yi, W.; Shen, X. L.; Li, Z. C.; Che, G. C.; Dong, X. L.; Sun, L. L.; Zhou, F.; Zhao, Z. X. *Europhys. Lett.* **2008**, *82*, 57002.
(6) Ren, Z. A.; Yang, J.; Lu, W.; Yi, W.; Che, G. C.; Dong, X. L.; Sun, L. L.; Zhao, Z. X. *Mater. Res. Innovations* **2008**, *12*(3), 105.
(7) Bos, J. W. G.; Penny, G. B. S.; Rodgers, J. A.; Sokolov, D. A.; Huxley, A. D.; Attfield, J. P. *Chem. Commun.* **2008**, *31*, 3634.
(8) Zhu, X.; Han, F.; Mu, G.; Cheng, P.; Shen, B; Zeng, B.; Wen, H. H. *Phys. Rev. B* **2009**, *79*, 220512(R).
(9) Ronnig, F.; Klimczuk, T.; Bauer, E. D.; Volz, H.; Thompson, J. D. *J. Phys.: Condens. Matter* **2008**, *20*, 322201.
(10) Tegel, M.; Rotter, M.; Weiss, V.; Shappacher, F. M.; Pottgen, R.; Johrendt, D. *J. Phys.: Condens. Matter* **2008**, *20*, 452201.
(11) Rotter, M.; Tegel, M.; Joherendt, D.; Schellenberg, I.; Hermes, W.; Pöttgen, R. *Phys. Rev. B* **2008**, *78*, 020503(R).
(12) Pitcher, M. J.; Parker, D. R.; Adamson, P.; Herkelrath, S. J. C.; Boothroyd, A. T.; Ibberson, R. M.; Brunelli, M.; Clarke, S. J. *Chem. Commun.* **2008**, *45*, 5918.
(13) Tapp, J. H.; Tang, Z.; Lv, B.; Sasmal, K.; Lorenz, B.; Chu, P. C. W.; Guloy, A. M. *Phys. Rev. B* **2008**, *78*, 060505(R).
(14) Wang, X. C.; Liu, Q. Q.; Lv, Y. X.; Gao, W. B.; Yang, L. X.; Yu, R. C.; Li, F. Y.; Jin, C. Q. *Solid State Commun.* **2008**, *148*, 538.
(15) Pitcher, M. J.; Lancaster, T.; Wright, J. D.; Franke, I.; Steele, A. J.; Baker, P. J.; Pratt, F. L.; Trevelyan Thomas, W.; Parker, D. R.; Blundell, S. J.; Clarke, S. J. *J. Am. Chem. Soc.* **2010**, *132*, 10467.
(16) Parker, D. R.; Pitcher, M. J.; Baker, P. J.; Franke, I.; Lancaster, T.; Blundell, S. J.; Clarke, S. J. *Chem. Commun.* **2009**, *16*, 2189.
(17) Parker, D. R.; Smith, M. J. P.; Lancaster, T.; Steele, A. J.; Franke, I.; Baker, P. J.; Pratt, F. L.; Pitcher, M. J.; Blundell, S. J.; Clarke, S. J. *Phys. Rev. Lett.* **2010**, *104*, 057007.

Published on Web 01/07/2011

order). If the structural variables (e.g., the shape of the $FeAs_4$ tetrahedra) are changed by isovalent substitution or by the application of an external pressure or if the electron count is changed by an aliovalent chemical substitution, then the magnetic instability is evaded and the stable ground state is a superconducting one. For example, at ambient pressure, $SrFe_2As_2$ or NaFeAs with fairly regular $FeAs_4$ tetrahedra can be doped into the superconducting regime by removing electrons as in $Sr_{1-x}K_xFe_2As_2$[18] or by direct doping on the Fe site as in $Sr(Fe_{1-x}Co_x)_2As_2$[19] or $NaFe_{1-x}Co_xAs$,[17] while LiFeAs with $FeAs_4$ tetrahedra which are highly compressed in the basal plane seems to be optimal in its undoped state.[15] In the case of $SrFe_2As_2$, doping is generally required to obtain superconductivity at ambient pressure although there are reports of superconductivity induced by hydrolysis in $SrFe_2As_2$ thin films[20] or, apparently, by defects in single crystals of $SrFe_2As_2$.[21] The precise effects of structure, electron count, and disorder on these compounds are complex and still emerging, and the details of the mechanism for superconductivity in these compounds are still under intense debate, but all these iron pnictides seem not to conform to the Bardeen-Cooper-Schrieffer (BCS) theory of superconductivity. Since the emergence of superconductivity in the iron arsenides is connected with the suppression of the magnetic order, it has been widely suggested that magnetic fluctuations may play an important role in the mechanism of superconductivity as is also assumed for the high-T_c cuprates.

In this paper, we describe the behavior of $SrFe_2As_2$ under Na-doping and investigate the interplay and competition between magnetic ordering and superconductivity. The synthesis, structure, and magnetic susceptibility measurements of the undoped "parent" material $SrFe_2As_2$ were first reported by Pfisterer et al. in 1980.[22] It crystallizes in the tetragonal $ThCr_2Si_2$-type structure in $I4/mmm$ at room temperature and exhibits a structural transition at 205 K to orthorhombic symmetry in $Fmmm$ (β-$SrRh_2As_2$-type). The structural phase transition is accompanied by an antiferromagnetic ordering transition, and the transitions in $SrFe_2As_2$ have been shown to be first order.[23,24] In common with most of the other layered iron arsenide systems, superconductivity may be induced in undoped $SrFe_2As_2$ by the application of hydrostatic pressure[25−28] or by electron or hole doping. The magnetic ordering present in $SrFe_2As_2$ is rapidly suppressed by substituting Fe by a range of other transition metals, and superconductivity emerges in $SrFe_{2-x}M_xAs_2$ (M = Co,[19] Ni,[29] and Rh, Ir, and Pd[30]) with maximum T_cs of 20 K in $SrFe_{1.8}Co_{0.2}As_2$ and 24 K in $SrFe_{1.57}Ir_{0.43}As_2$. This behavior of the iron arsenides contrasts with the cuprate superconductors where substitutions on the Cu site lead to rapid suppression of superconductivity with increased doping. Substitution of the alkaline-earth metals by alkali metals leads to hole doping in the AFe_2As_2 "122" compounds producing superconductors.[18,31−36] Complete solid solutions $Sr_{1-x}K_xFe_2As_2$ and $Sr_{1-x}Cs_xFe_2As_2$ are available, and the end members adopt the same structure type. In $Sr_{1-x}K_xFe_2As_2$, T_c increases with doping to a maximum of about 37 K for $x = 0.5-0.6$ and decreases toward the KFe_2As_2 end member, in which superconductivity persists only at very low temperatures.[18] Only the very Sr-rich members are not superconductors.

However, while KFe_2As_2 adopts the $ThCr_2Si_2$-type structure with K^+ in 8-coordination by As, this square prismatic site is too large for Na: $NaFe_2As_2$ may be formed at low temperatures but is a metastable compound.[37] Substitution of the alkaline earth by Na^+ has been reported in $Ca_{1-x}Na_xFe_2As_2$, $Ba_{1-x}Na_xFe_2As_2$, and $Eu_{1-x}Na_xFe_2As_2$.[31,32,34,36] However, the full solid solutions cannot be stabilized, and the reported limits are $x = 0.5$, 0.6, and 0.3 for the Ca, Ba, and Eu cases, respectively. In $Ba_{1-x}Na_xFe_2As_2$, the regime of optimal superconductivity ranges from $x = 0.4$ to the phase limit at $x = 0.6$.[34]

Here, we contrast the Na-doping of $BaFe_2As_2$, the K-doping of $SrFe_2As_2$, and the alkali metal doping of other 122 parent compounds with a new series of superconductors obtained by the Na-doping of $SrFe_2As_2$. The compositional range for pure $Sr_{1-x}Na_xFe_2As_2$ compositions is $0 \le x \le 0.4$ and while superconductivity is observed in the compositions approaching the compositional limit the competing magnetic ordering is never quite suppressed in these samples.

Experimental Section

All manipulations were carried out in a Glovebox Technology argon-filled glovebox. Samples of nominal composition

(18) Sasmal, K.; Lv, B.; Lorenz, B.; Guloy, A. M.; Cheng, F.; Xue, Y.-Y; Chu, C.-W. *Phys. Rev. Lett.* **2008**, *101*, 107007.
(19) Leithe-Jasper, A.; Schnelle, W.; Geibel, C.; Rosner, H. *Phys. Rev. Lett.* **2008**, *101*, 207004.
(20) Hiramatsu, H.; Katase, T.; Kamiya, T.; Hirano, M.; Hosono, H. *Phys. Rev. B* **2009**, *80*, 052501.
(21) Saha, S. R.; Butch, N. P.; Kirshenbaum, K.; Paglione, J. *Phys. Rev. Lett.* **2009**, *103*, 037005.
(22) Pfisterer, M.; Nagorsen, G. Z. *Naturforsch. B* **1980**, *35B*, 703.
(23) Krellner, C.; Caroca-Canales, N.; Jesche, A.; Rosner, H.; Ormeci, A.; Geibel, C. *Phys. Rev. B* **2008**, *78*, 100504(R).
(24) Loudon, J. C.; Bowell, C. J.; Gillett, J.; Sebastian, S. E.; Midgley, P. A. *Phys. Rev. B* **2010**, *81*, 214111.
(25) Kumar, M.; Nicklas, M.; Jesche, A.; Caroca-Canales, N.; Schmitt, M.; Hanfland, M.; Kasinathan, D.; Schwarz, U.; Rosner, H.; Geibel, C. *Phys. Rev. B* **2008**, *78*, 184516.
(26) Torikachvili, M. S.; Bud'ko, S. L.; Ni, N.; Canfield, P. C. *Phys. Rev. B* **2008**, *78*, 104527.
(27) Alireza, P. L.; Gillett, J.; Ko, Y. T. C.; Sebastian, S. E.; Lonzarich, G. G. *J. Phys.: Condens. Matter* **2009**, *21*, 012208.
(28) Colombier, E.; Bud'ko, S. L.; Ni, N.; Canfield, P. C. *Phys. Rev. B* **2009**, *79*, 224518.
(29) Saha, S. R.; Butch, N. P.; Kirshenbaum, K.; Paglione, J. *Phys. Rev. B* **2009**, *79*, 224519.
(30) Han, F.; Zhu, X.; Cheng, P.; Mu, G.; Jia, Y.; Fang, L.; Wang, Y; Luo, H.; Zeng, B.; Shen, B.; Shan, L.; Ren, C.; Wen, H. H. *Phys. Rev. B* **2009**, *80*, 024506.
(31) Shirage, P. M.; Miyazawa, K.; Kito, H.; Eisaki, H.; Iyo, A. *Appl. Phys. Express* **2008**, *1*, 081702.
(32) Wu, G.; Chen, H.; Wu, T.; Xie, Y. L.; Yan, Y. J.; Liu, R. H.; Wang, X. F.; Ying, J. J.; Chen, X. H. *J. Phys.: Condens. Matter* **2008**, *20*, 422201.
(33) Rotter, M.; Pangerl, M.; Tegel, M.; Joherendt, D. *Angew. Chem., Int. Ed.* **2008**, *47*, 7949.
(34) Cortes-Gil, R.; Paker, D. R.; Pitcher, M. J.; Hadermann, J.; Clarke, S. J. *Chem. Mater.* **2010**, *22*(14), 4304.
(35) Jeevan, H. S.; Hossain, Z.; Kasinathan, D.; Rosner, H.; Geibel, C.; Gegenwart, P. *Phys. Rev. B* **2008**, *78*, 092406.
(36) Qi, Y.; Gao, Z; Wang, L.; Wang, D.; Zhang, X.; Ma, Y. *New J. Phys.* **2008**, *10*, 123003.
(37) Gooch, M.; Lv. B.; Sasmal, K.; Tapp, J. H.; Tang, Z. J.; Guloy, A. M.; Lorenz, B.; Chu, C. W. Phys. C **2009**, DOI: 10.1016/j.physc.2009.10.096.

$Sr_{1-x}Na_xFe_2As_2$ ($0 \le x < 0.8$) were synthesized by heating stoichiometric mixtures of the elements. Sr (rods, Aldrich 99%) was sublimed under high vacuum at 850 °C prior to use. Na lump (BDH 99.9%) and Fe powder (ALFA 99.998%) were used as received, and As pieces (ALFA 99.9999%) were pulverized prior to use. Fe and As powders were ground together and added to appropriate amounts of Na and Sr pieces in Nb tubes which were then sealed by welding in an arc furnace under 1 atm argon gas and then sealed in protective evacuated silica tubes. The mixtures were heated at 1 °C min^{-1} to 800 °C. This temperature was maintained for 3 days, and the reaction vessels were then cooled rapidly to room temperature by removing them from the hot furnace. After homogenization in an agate mortar inside the glovebox, the products were pressed into 13 mm diameter pellets, sealed in a second Nb tube, and then annealed at 900 °C for 30 h, and once again, cooled rapidly to room temperature. The compounds are black with metallic luster and are inert to air and moisture for at least several weeks according to analysis using laboratory powder X-ray diffraction measurements.

Phase identification and crystal structure investigation were carried out by X-ray powder diffraction (XRPD) using a PANalytical X′pert PRO diffractometer operating with Cu $K\alpha_1$ radiation in Bragg−Brentano geometry at room temperature. High-resolution XRPD was performed at ambient and low temperatures on the beamline ID31 at the ESRF, Grenoble using 0.4 Å X-rays. Neutron powder diffraction (NPD) patterns at ambient and low temperatures were collected on the diffractometers D2B (ILL, Grenoble), POLARIS, OSIRIS, and HRPD (ISIS, UK) with the samples contained in thin-walled vanadium cylinders. Crystal and magnetic structures were refined by the Rietveld method using the GSAS suite of programmes[38] via the EXPGUI interface.[39] In order to characterize the superconducting and magnetic properties, zero-field-cooled (ZFC) and field-cooled (FC) magnetization measurements were performed from 2 to 300 K in a measuring field of 50 Oe using a SQUID magnetometer (Quantum Design, MPMS-XL).

Results and Discussion

Samples of $Sr_{1-x}Na_xFe_2As_2$ with $x \le 0.42$ appeared single phase according to laboratory XRPD measurements. Attempts to prepare materials richer in Na, i.e., $Sr_{0.56}Na_{0.44}Fe_2As_2$, resulted in the clear formation of NaFeAs impurity phase (Figure S2, Supporting Information). Samples with compositions even richer in Na (i.e., $Sr_{0.5}Na_{0.5}Fe_2As_2$, $Sr_{0.46}Na_{0.54}Fe_2As_2$, $Sr_{0.4}Na_{0.6}Fe_2As_2$, $Sr_{0.3}Na_{0.7}Fe_2As_2$, $Sr_{0.2}Na_{0.8}Fe_2As_2$) produced additional impurities of Fe, Fe_2As, and Na_3As. Subsequent examination of the sample $Sr_{0.58}Na_{0.42}Fe_2As_2$ using higher quality synchrotron XRPD and NPD data revealed approximately 1% by mass of elemental iron in this sample (Figure S1, Supporting Information), but no additional impurities were evident; we elaborate on this point below. Goko et al.[40] described muon spin-relaxation measurements on a 40 mg single crystal grown from a FeAs flux with a nominal composition of $Sr_{0.5}Na_{0.5}Fe_2As_2$ with $T_c = 35$ K (from susceptibility measurements). However, no complementary structural or compositional information was supplied for this sample. Despite multiple attempts using synthesis temperatures from 700 to 900 °C and slow cooling or rapid quenching from the furnace, we could not obtain single phase bulk powder samples using our methods for $x = 0.5$; although in light of the existence of metastable $NaFe_2As_2$,[37] we cannot rule out that the formation of more sodium-rich compositions of $Sr_{1-x}Na_xFe_2As_2$ with $x > 0.4$ are possible.

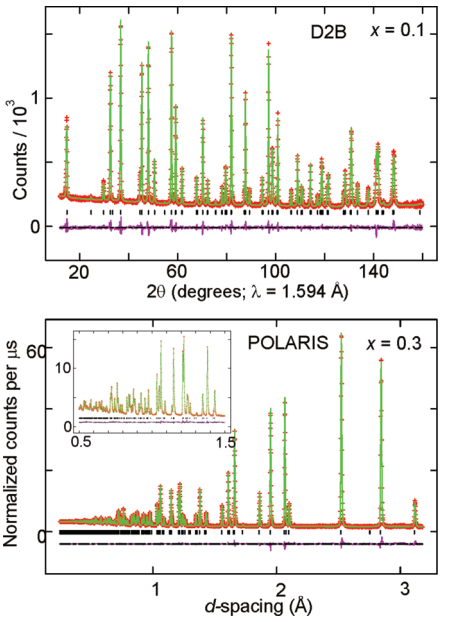

Figure 1. Rietveld refinements against D2B or POLARIS (145° data bank) data for the samples $Sr_{1-x}Na_xFe_2As_2$ with $x = 0.1$ and 0.3 ($x = 0.1$ (D2B), $R_{wp} = 0.0355$, $R_{F2} = 0.0217$, $\chi^2 = 2.967$, 22 variables; $x = 0.3$ (POLARIS), $R_{wp} = 0.0176$, $R_{F2} = 0.131$, $\chi^2 = 1.99$).

Table 1. Lattice Parameters of $Sr_{1-x}Na_xFe_2As_2$ from Laboratory PXRD Data at Room Temperature

x	a (Å)	c (Å)	V (Å^3)
0	3.92430	12.36440	190.413
0.1	3.91680(4)	12.4205(1)	190.547(5)
0.2	3.90682(9)	12.4583(4)	190.15(1)
0.3	3.90207(6)	12.4787(2)	190.003(9)
0.35	3.89309(5)	12.5093(2)	189.593(8)
0.37	3.8842(1)	12.5348(5)	189.12(2)
0.4	3.87950(4)	12.5534(2)	188.935(7)
0.42[a]	3.88774(9)	12.5354(4)	189.47(1)

[a] Denotes impure sample.

Room Temperature Crystal Structures

The trends in the crystal structures of the compounds $Sr_{1-x}Na_xFe_2As_2$ were determined by Rietveld refinements against XRPD and NPD data (Figure 1). All of them crystallize at room temperature in the tetragonal $ThCr_2Si_2$-type structure with space group $I4/mmm$. Table 1 shows the variation of the lattice parameters with sodium content from laboratory XRPD data. The basal lattice parameter, a, which is directly proportional to the Fe−Fe distance ($a = (2)^{1/2} \times$ (Fe−Fe)) shows a general decrease

(38) Larson, A. C.; Von Dreele, R. B. *General Structure Analysis System (GSAS)*, Los Alamos National Laboratory Report LAUR 86-748; Los Alamos National Laboratory: Los Alamos, NM, U.S.A., 2004.
(39) Toby, B. H. *J. Appl. Crystallogr.* **2001**, *34*, 210.
(40) Goko, T.; Aczel, A. A.; Baggio-Saitovitch, E.; Bud'ko, S. L.; Canfield, P. C.; Carlo, J. P.; Chen, G. F.; Dai, P. C.; Hamann, A. C.; Hu, W. Z.; Kageyama, H.; Luke, G. M.; Luo, J. L.; Nachumi, B.; Ni, N.; Reznik, D.; Sanchez-Candela, D. R.; T. Savici, A.; Sikes, K. J.; Wang, N. L.; Wiebe, C. R.; Williams, T. J.; Yamamoto, T.; Yu, W.; Uemura, Y. J. *Phys. Rev. B* **2009**, *80*, 024508.

with increasing sodium concentration (i.e., increasing x and decreasing electron count) while the c axis perpendicular to the FeAs layers shows a general increase with increasing x in the range $0 \leq x \leq 0.4$. The cell volume decreases because the elongation of the c axis is more than compensated by the significant decrease of the a axis, and this is consistent with the smaller ionic radius of Na^+ than Sr^{2+}.[41] For the sample with $x = 0.42$, which lies just beyond the single phase region, the trends in the behavior of the a and c axes seem to reverse, and the unit cell volume increases slightly for this Na content; it has very similar lattice parameters to the sample with $x = 0.35$, but the low temperature behavior of these two samples is quite different (see below). Refinements of the Na/Sr ratio in the samples (neutron scattering lengths are Sr: 7.02 fm; Na: 3.63 fm) produced compositions corresponding to the nominal compositions within the uncertainty arising from correlations between site occupancy factors and atomic displacement parameters in the Rietveld refinements (Table 1 and Table S4, Supporting Information). This is in accord with the single phase nature of these samples which were prepared in sealed vessels.

As described above, the high-resolution XRPD data (ID31; Figure S1, Supporting Information) and medium resolution NPD data (POLARIS) for $Sr_{0.58}Na_{0.42}Fe_2As_2$ revealed the existence of elemental Fe. Rietveld analysis of the data revealed 1% by mass of iron in the sample but no additional impurities. However, no corresponding small deficiency of iron in the ternary arsenide phase was evident from the refinements. The presence of elemental iron for $x = 0.42$ suggests that this sample is just beyond the phase limit of the $Sr_{1-x}Na_xFe_2As_2$ series.

Detailed structural data for the $Sr_{1-x}K_xFe_2As_2$ solid solution[18] have not been reported. Recently,[34] we showed that the behavior of the basal lattice parameter with composition in the $Ba_{1-x}Na_xFe_2As_2$ series ($0 \leq x \leq 0.6$) was quantitatively similar to that in the $Ba_{1-x}K_xFe_2As_2$ series showing that electron count is the key factor controlling the basal lattice parameter ($(2)^{1/2} \times$ Fe−Fe). If we compare the behavior of the $Sr_{1-x}Na_xFe_2As_2$ series with that of the $Ba_{1-x}Na_xFe_2As_2$ series,[34] we see that the trends in the basal lattice parameter are fairly similar (Figure 2); they are not expected to be identical because of the difference in basal lattice parameters of the undoped $AeFe_2As_2$ parent phases. The changes in c and V with x are greater in the $Ba_{1-x}Na_xFe_2As_2$ series than in the $Sr_{1-x}Na_xFe_2As_2$ series which presumably reflects the greater size-mismatch between Ba^{2+} and Na^+ than between Sr^{2+} and Na^+.[41]

Table 2 shows the variation of the room temperature structural parameters of $Sr_{1-x}Na_xFe_2As_2$ obtained from refinements against NPD data. While the Fe−Fe bond length which is trivially related to the lattice parameter a ($a = (2)^{1/2} \times$ Fe−Fe) decreases with increasing x, the Fe−As distance is almost invariant with x. The $FeAs_4$ tetrahedra, therefore, become more elongated along the c axis. As the smaller Na^+ is substituted for Sr^{2+}, the Sr/Na−As distance decreases with x only about half as rapidly as the basal lattice parameter (equal to the intralayer As−As distance) decreases, with the consequence that the interlayer As−As distance increases slightly with increasing sodium content. The net result of the decrease of a and the bond length changes is that c increases. The $FeAs_4$ tetrahedra in $SrFe_2As_2$ are very slightly compressed along the c direction. As x increases, the As−Fe−As angles take the ideal tetrahedra angle of 109.5° at around $x = 0.2$, and thereafter, the tetrahedra become slightly elongated along c (Figure 3, Table 2). It has been observed empirically that within a series of arsenide superconductors regular tetrahedra generally favor high values of T_c providing the electron count is optimized.[42]

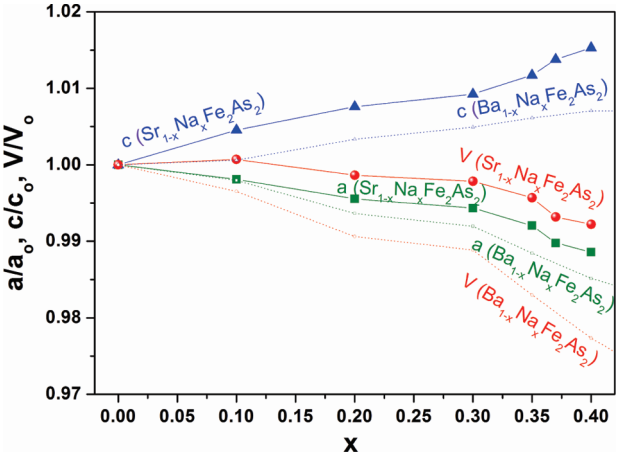

Figure 2. Evolution at room temperature of the lattice parameters and unit cell volume of $Sr_{1-x}Na_xFe_2As_2$ as a function of x, compared with the corresponding evolution in $Ba_{1-x}Na_xFe_2As_2$.[34] Values are given as fractions of the values in the corresponding $AeFe_2As_2$ phases.

Low Temperature Crystal Structures

Figure 4 shows the experimental and fitted NPD pattern of $Sr_{0.7}Na_{0.3}Fe_2As_2$ collected at 5 K on the diffractometer OSIRIS (ISIS). It was indexed with an orthorhombic β-$SrRh_2As_2$-type structure with space group $Fmmm$. The inset to Figure 4 shows the well-resolved splitting of the tetragonal (112), (114), and (213) reflections. In the general phase diagram for the iron arsenide systems, the orthorhombic distortion and the size of the long-range ordered magnetic moment are suppressed as the systems enter the superconducting regime. There is much debate about the nature of the compounds in the region of compositions where magnetic order and superconductivity are observed to coexist. Some local probe measurements (Mössbauer spectroscopy[43] and NMR spectroscopy) suggest that the coexistence is microscopic in at least some systems with all Fe atoms participating both in magnetic

(41) Shannon, R. D.; Prewitt, C. T. *Acta Crystallogr., Sect. B* **1969**, *25*, 925.

(42) Lee, C. H.; Iyo, A.; Eisaki, H.; Kito, H.; Fernandez-Diaz, M. T.; Ito, T.; Kihou, K.; Matsuhata, H.; Braden, M.; Yamada, K. *J. Phys. Soc. Jpn.* **2008**, *77*, 083704.

(43) Rotter, M.; Tegel, M.; Schellenberg, I.; Schappacher, F. M.; Pottgen, R.; Deisenhofer, J.; Gunther, A.; Schrettle, F.; Loidl, A.; Johrendt, D. *New J. Phys.* **2009**, *11*, 025014.

Table 2. Refined Atomic Parameters, Bond Distances, and Bond Angles for $Sr_{1-x}Na_xFe_2As_2$ from NPD Data at Room Temperature[a]

x	0[b]	0.1[c]	0.2[c]	0.3[d]	0.37[c]	0.4[c]	0.42[c,e]
$10^4 \times$ (Sr/Na U_{iso} (Å^2))	129(5)	115(2)	117(4)	107(2)	118(5)	151(5)	136(5)
$10^4 \times$ (Fe U_{iso} (Å^2))	72(4)	81(1)	88(2)	81(1)	59(2)	77(2)	92(3)
As z	0.3600(1)	0.36099(8)	0.3611(1)	0.36107(2)	0.36157(9)	0.36164(9)	0.3615(1)
$10^4 \times$ (As U_{iso} (Å^2))	86(4)	99(2)	99(3)	76(1)	74(3)	90(3)	116(4)
Fe−Fe (Å) [4][f]	2.775(1)	2.77181(3)	2.76166(3)	2.75700(4)	2.74463(4)	2.74132(3)	2.74973(5)
Fe−As (Å) [4][f]	2.388(1)	2.3969(5)	2.3932(7)	2.3910(3)	2.3915(7)	2.3913(7)	2.3949(7)
Sr/Na−As (Å) [8][f]	3.270(1)	3.2663(5)	3.2586(7)	3.2559(3)	3.2464(6)	3.2446(6)	3.2519(7)
As−As (Å) [1][f]	3.462(3)	3.456(5)	3.459(2)	3.464(8)	3.468(2)	3.471(2)	3.472(2)
As−Fe−As (°) [2][f]	110.5(1)	109.72(4)	109.37(5)	109.25(2)	108.49(5)	108.31(5)	108.56(5)
As−Fe−As (°) [4][f]	108.9(1)	109.35(2)	109.52(2)	109.59(1)	109.97(2)	110.06(2)	109.93(3)

[a] Space Group: *I*4/*mmm* (No.139). Sr,Na: 2*a* (0,0,0), Fe: 4*d* (1/2,0,1/4), As 4*e* (0,0,*z*). Refinements were performed using the nominal value of the Sr/Na ratio as correlation between the occupancy factor and the displacement parameter for the Sr/Na site resulted in uncertainty of about 5% in the value of the scattering at the Sr/Na site. See Table S4 (Supporting Information) and the accompanying note. [b] Ref 10. [c] D2B (ILL). [d] POLARIS (ISIS). [e] Impure sample (1% Fe impurity). [f] Numbers in square brackets denote the multiplicity of each bond or angle.

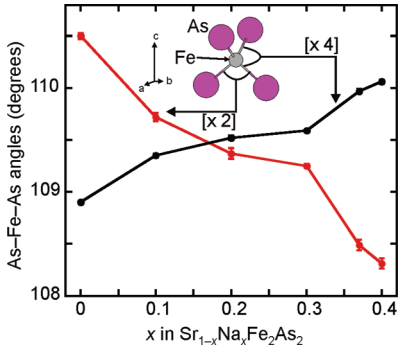

Figure 3. Evolution of bond angles in the $FeAs_4$ tetrahedron of $Sr_{1-x}Na_x$-Fe_2As_2 compounds at room temperature.

ordering and in superconductivity. The alternative picture is that there is genuine phase separation into mesoscopic regions of magnetically ordered and superconducting material. X-ray and neutron diffraction methods are inherently a probe of the long-range average structure, so they are unable to distinguish between phase separation into regions smaller than several hundred nanometers or microscopic coexistence. According to our low temperature diffraction measurements, the samples are single phase at low temperatures. Table 3 shows the 5 K lattice parameters as a function of x in $Sr_{1-x}Na_xFe_2As_2$ in the range $0 \le x \le 0.42$. A summary of the crystallographic data at 5 K for $Sr_{1-x}Na_xFe_2As_2$ samples is compiled in the Supporting Information (Tables S1−S3).

The orthorhombic distortion in $SrFe_2As_2$ is the largest measured among the iron pnictide systems. In the $Sr_{1-x}Na_xFe_2As_2$ series the distortion is well resolved as far as $x = 0.35$, similar to the observations in the $Ba_{1-x}Na_xFe_2As_2$ and $Ba_{1-x}K_xFe_2As_2$ series. In the Sr_{1-x}-$Na_xFe_2As_2$ series, there is a just-discernible peak broadening at low temperatures at $x = 0.40$ on HRPD, but for the $x = 0.42$ composition which contained a small Fe impurity, there is no clear evidence for a structural distortion even using the highest resolution diffractometer available (ID31) although there is a small change in the shapes of peaks which would split on orthorhombic distortion (Figure 5a) suggesting that the distortion occurs to a tiny extent. The changes in peak shape are

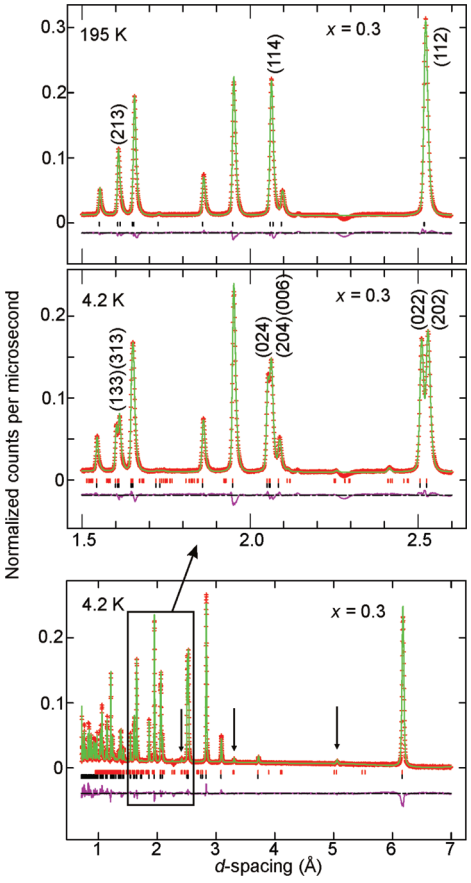

Figure 4. NPD pattern (OSIRIS) and Rietveld fit of $Sr_{0.7}Na_{0.3}Fe_2As_2$ at 4.2 K with magnetic Bragg peaks indicated ($R_{wp} = 0.0669$). Tetragonal and orthorhombic reflections at 195 and 5 K are compared for a selected region on the patterns.

similar to those found in $NaFe_{0.975}Co_{0.025}As$ which lies well into the superconducting regime in the $NaFe_{1-x}$-Co_xAs system.[17]

The highest resolution data collected on HRPD for $Sr_{0.7}Na_{0.3}Fe_2As_2$ shows that reflections related to the tetragonal phase coexist with reflections related to the orthorhombic phase at 160 K as shown in Figure 6. By 170 K, the (022) and (202) reflections of the orthorhombic low temperature phase have been completely replaced by the (112) reflection of the tetragonal high temperature phase. This shows that the structural transition in doped

Table 3. Lattice Parameters of $Sr_{1-x}Na_xFe_2As_2$ from NPD Data at 5 K[a]

x	a (Å)	b (Å)	c (Å)	V (Å^3)
0[b]	5.5783(3)	5.5175(3)	12.2965(6)	378.46(6)
0.1[c]	5.56699(7)	5.50871(7)	12.3260(2)	378.00(1)
0.2[c]	5.54706(7)	5.49349(7)	12.3327(2)	375.81(2)
0.3[d]	5.5392(1)	5.4882(1)	12.3460(6)	375.32(3)
0.35[d]	5.52191(9)	5.48344(9)	12.4183(2)	376.02(2)
0.4[d]	5.4869(2)	5.4828(2)	12.4216(2)	373.68(3)
0.42[c]	3.88556(7)		12.4006(3)	187.22(1)

[a] $0 \le x \le 0.4$: Space Group *Fmmm* (No.69). Sr,Na: *2a* (0,0,0), Fe: *8f* (1/4,1/4,1/4), As *8i* (0,0,*z*); $x = 0.42$: Space Group: *I4/mmm* (No.139). Sr,Na: *2a* (0,0,0), Fe: *4d* (1/2,0,1/4), As *4e* (0,0,z). [b] Ref 10. [c] D2B (ILL). [d] HRPD(ISIS).

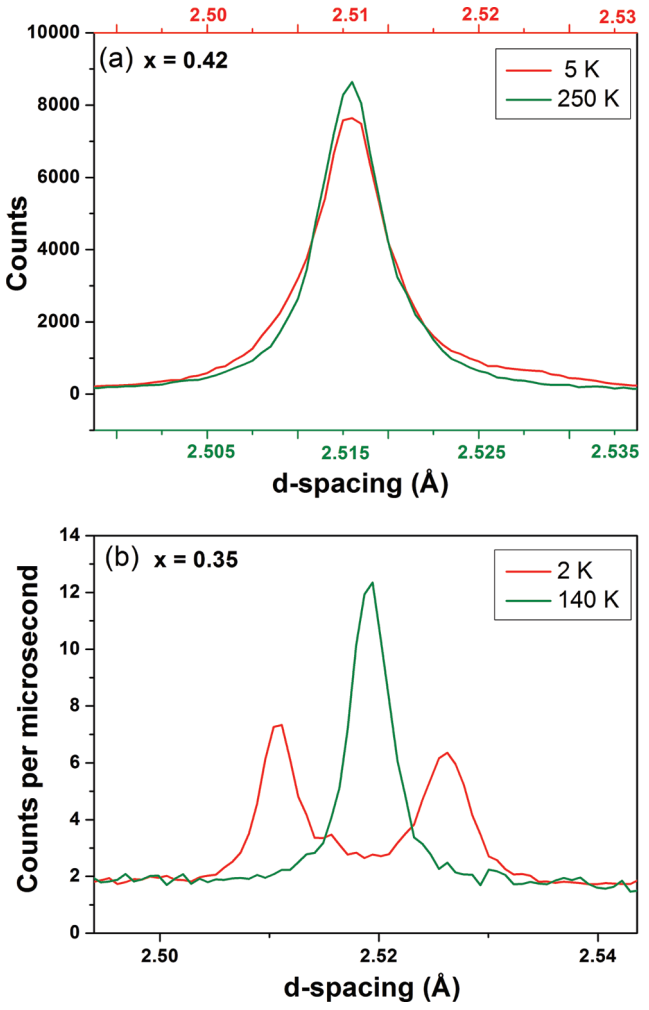

Figure 5. (a) High resolution synchrotron pattern of $Sr_{0.58}Na_{0.42}Fe_2As_2$ at 5 and 250 K collected on ID31 (ESRF). (b) High resolution neutron diffraction patterns of $Sr_{0.65}Na_{0.35}Fe_2As_2$ at 2 and 140 K collected on HRPD (ISIS).

$SrFe_2As_2$ compounds is first order which has been confirmed by microscopic investigations of the phase transition in $SrFe_2As_2$.[24]

Magnetic Ordering

The structural phase transition in $SrFe_2As_2$ and the other "parent" materials are driven by an antiferromagnetic ordering transition. The strong coupling between the structural and magnetic order is again a clear evidence

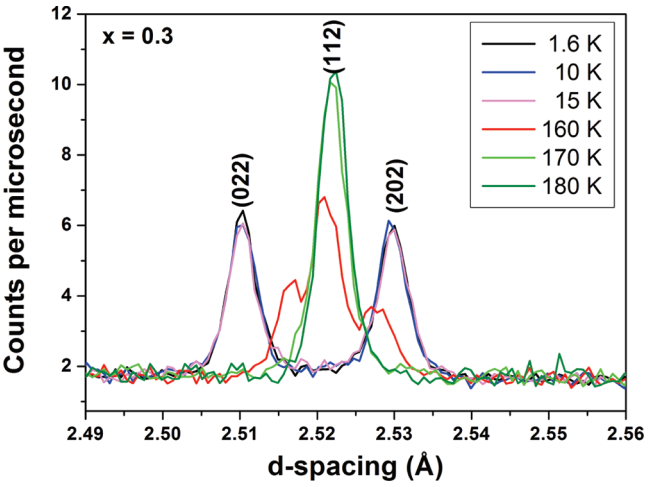

Figure 6. Temperature dependence (112) reflections as a function of temperature in $Sr_{0.7}Na_{0.3}Fe_2As_2$ collected on HRPD.

for a first order transition.[23] Suppression of the antiferromagnetic order and the orthorhombic distortion by doping (or by the application of pressure) appears to be what allows a bulk superconducting ground state to be favored. Figure 7 shows the NPD data from OSIRIS on $Sr_{0.65}Na_{0.35}Fe_2As_2$. The resolution is poorer than on HRPD which makes it hard to tell whether the orthorhombic and tetragonal phases coexist. Magnetic Bragg peaks are evident which appear on cooling at about the same temperature as the orthorhombic distortion, in line with the behavior of $SrFe_2As_2$.[23]

In the $Sr_{1-x}Na_xFe_2As_2$ series, Bragg peaks due to antiferromagnetic ordering of moments located on Fe are evident in the 5 K neutron diffractogram for all members of the series $0 \le x \le 0.42$, i.e., including the sample with $x = 0.42$ which contains a small Fe impurity and shows no resolvable orthorhombic distortion. The magnetic propagation vector of $Sr_{1-x}Na_xFe_2As_2$ is $\mathbf{q} = (1\ 0\ 1)$[44] with the Fe magnetic moments aligned antiferromagnetically both along the longer *a* direction in the basal plane and between layers and aligned ferromagnetically along the shorter *b* axis in the basal plane. The magnetic ordering within the FeAs layers is similar to that in $BaFe_2As_2$[45] and LnFeAs(O,F).[46,47]

The refined magnetic moments are plotted together with the size of the orthorhombic distortion in Figure 8a, and the corresponding data for $Ba_{1-x}Na_xFe_2As_2$ are given in Figure 8b for comparison. An unusual feature of the $Sr_{1-x}Na_xFe_2As_2$ system is that, in the sample with $x = 0.42$ which contains a small elemental Fe impurity, long-range magnetic order is still evident in the ternary phase but the structural phase transition seems to have been

(44) Kaneko, K.; Hoser, A.; Caroca-Canales, N.; Jesche, A.; Krellner, C.; Stockert, O; Geibel, C. *Phys. Rev. B* **2008**, *78*, 212502.
(45) Huang, Q.; Qiu, Y.; Bao, W.; Green, M. A.; Lynn, J. W.; Gasparovic, Y. C.; Wu, T.; Wu, G.; Chen., X. H. *Phys. Rev. Lett.* **2008**, *101*, 257003.
(46) De la Cruz, C.; Huang, Q.; Lynn, J. W.; Li, J.; Ratcliff, W., II; Zarestky, J. L.; Mook, H. A.; Chen, G. F.; Luo, J. L.; Wang, N. L.; Dai, P. *Nature* **2008**, *453*, 899.
(47) Zhao, J.; Huang, Q.; de la Cruz, C.; Li, S. L.; Lynn, J. W.; Chen, Y.; Green, M. A.; Chen, G. F.; Li, G.; Li, Z.; Luo, J. L.; Wang, N. L.; Dai., P. C. *Nat. Mater.* **2008**, *7*, 953.

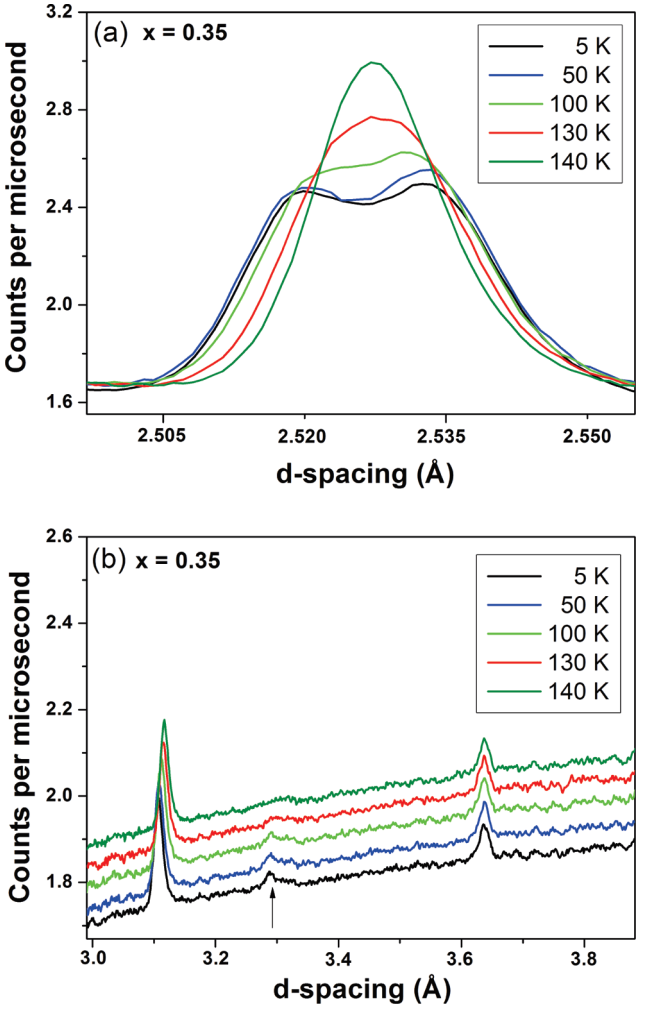

Figure 7. (a) Temperature dependence of the tetragonal(112)/orthorhombic(022)/(202) reflections for $Sr_{0.65}Na_{0.35}Fe_2As_2$ and (b) the evolution of the magnetic (103) reflection in $Sr_{0.65}Na_{0.35}Fe_2As_2$. Data collected on OSIRIS.

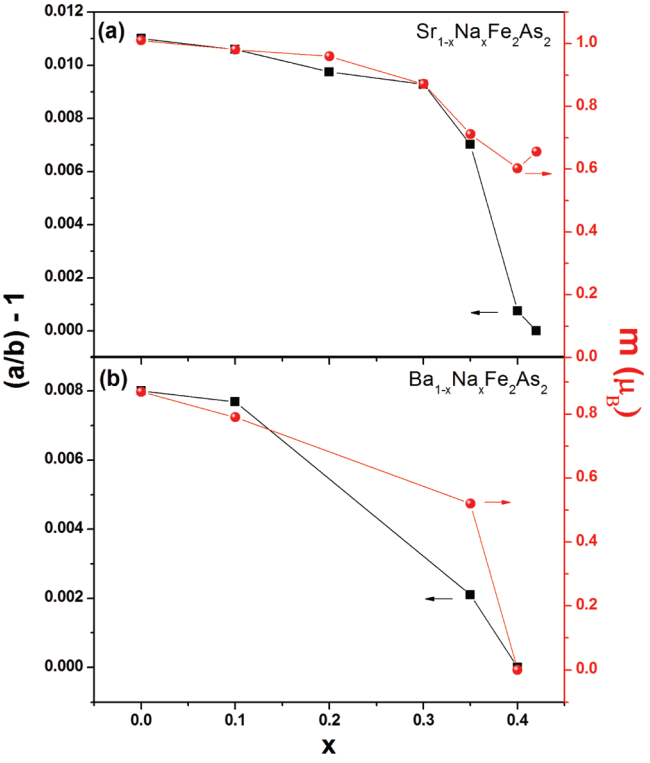

Figure 8. Variation of the orthorhombic distortion and ordered magnetic moment at 5 K in (a) $Sr_{1-x}Na_xFe_2As_2$ and (b) $Ba_{1-x}Na_xFe_2As_2$. Data for $Ba_{1-x}Na_xFe_2As_2$ are from ref 34.

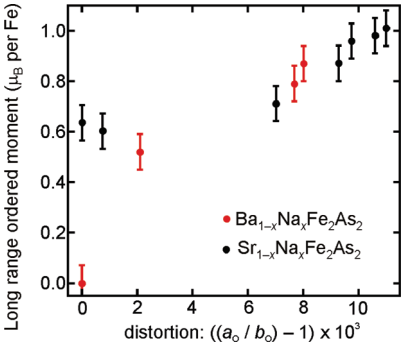

Figure 9. Correlation between the size of the orthorhombic distortion quantified by the ratio of the basal orthorhombic lattice parameters and the size of the ordered magnetic moment for a series of Na-doped 122 iron arsenides.

completely suppressed: 5 K NPD data from D2B for $x = 0.42$ show no evidence for peak broadening, yet the refined moment is similar to the value in $Sr_{0.65}Na_{0.35}Fe_2As_2$. Indeed, on the basis of the room temperature lattice parameters, $Sr_{0.65}Na_{0.35}Fe_2As_2$ and $Sr_{0.58}Na_{0.42}Fe_2As_2$ seem similar, but their low temperature behaviors are quite different; their refined compositions correspond to the nominal ones (Table S4, Supporting Information). The comparison is shown in Figure 5 where portions of the diffraction patterns for $Sr_{0.58}Na_{0.42}Fe_2As_2$ at 5 and 250 K (ID31) and $Sr_{0.65}Na_{0.35}Fe_2As_2$ at 2 and 140 K (HRPD) are shown.

Our measurements show that $Sr_{0.7}Na_{0.3}Fe_2As_2$ exhibits a larger orthorhombic distortion than the isoelectronic composition in the $Ba_{1-x}Na_xFe_2As_2$ series (Figure 8a,b); in $Ba_{0.7}Na_{0.3}Fe_2As_2$, only broadening of the $(112)_T$ reflection of the tetragonal phase is evident.[34] The results also show that, while the size of the ordered moment on the Fe atoms in the itinerant antiferromagnets $SrFe_2As_2$ and $BaFe_2As_2$ both decrease on Na doping, the values of the ordered moment in the members of the $Sr_{1-x}Na_xFe_2As_2$ series are higher than for isoelectronic members of the $Ba_{1-x}Na_xFe_2As_2$ series. In the undoped compounds, the ordered moments per Fe ion are as follows: 1.01(3) μ_B in $SrFe_2As_2$[44] and 0.87(3) μ_B in $BaFe_2As_2$[45] determined using neutron powder diffraction measurements. Figure 9 shows that there is a strong correlation between the size of the ordered moment and the size of the distortion for these compounds.

Magnetic Susceptibility Measurements

The magnetic susceptibility measurements show no clear signature of antiferromagnetic ordering (Figure S3, Supporting Information), but these measurements were used to determine the effect of Na doping on superconductivity. Zero-field cooled (ZFC) and field cooled (FC) measurements were carried out in applied field of 50 Oe. No demagnetization corrections were applied, but all the

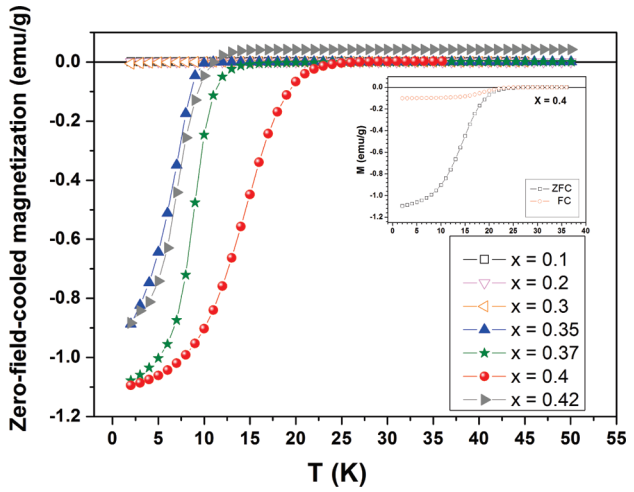

Figure 10. ZFC magnetization for $Sr_{1-x}Na_xFe_2As_2$. The inset shows ZFC and FC data for $x = 0.4$. The iron impurity in the sample with $x = 0.42$ is evident in the enhanced normal state susceptibility relative to the other samples. The $x = 0.3$ sample shows a very small superconducting volume fraction (see Figure S3, Supporting Information).

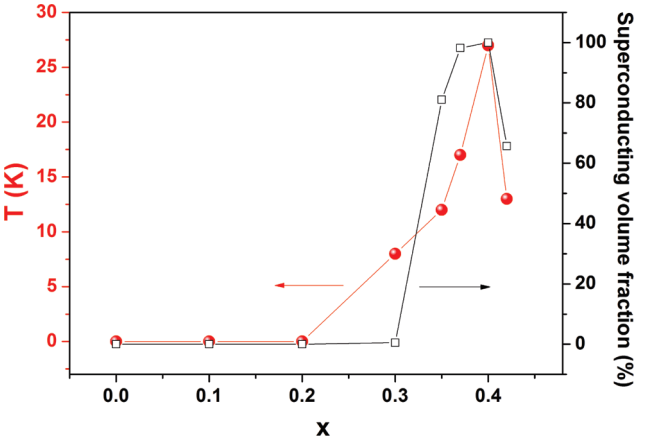

Figure 11. Phase diagram of $Sr_{1-x}Na_xFe_2As_2$ with the critical temperature and superconducting volume fraction as a function of the sodium concentration. The sample with $x = 0.42$ is included, but this sample contains an elemental iron impurity and lies outside the single phase region.

samples were of similar mass and shape. For clarity, only ZFC measurements are shown for all samples in Figure 10 with both ZFC and FC measurements displayed for $Sr_{0.6}Na_{0.4}Fe_2As_2$ in the inset, showing the Meissner effect. All samples with $x \geq 0.3$ display superconductivity. This is in agreement with the behavior of the $Sr_{1-x}K_xFe_2As_2$ solid solution in which superconductivity appears for $x > 0.1$.[18] Na and K doping in $BaFe_2As_2$ induce superconductivity at slightly lower hole concentrations with superconductivity first evident at $x = 0.1$.[34] It seems plausible that one reason for this is the apparently more robust antiferromagnetically ordered state present in the Sr case. Note that the sample with $x = 0.3$ exhibits a broad superconducting transition but with a very small superconducting volume fraction (see Figure S3, Supporting Information).

In the $Sr_{1-x}Na_xFe_2As_2$ series, the maximum value of superconductivity at 26 K is exhibited at $x = 0.4$. This is the limiting phase pure composition which we have identified using our synthetic methods. The sample with $x = 0.42$ which contains a small Fe impurity has a lower T_c. In the other solid solutions derived from $SrFe_2As_2$ and $BaFe_2As_2$ by doping with alkali metals, this composition marks the start of a superconducting "dome" that is broad in composition. Unusually, the $Sr_{1-x}Na_xFe_2As_2$ series seems very close to the phase limit at $x = 0.4$, so no broad "dome" is evident. Figure 11 shows the superconducting critical temperature, as well as estimated superconducting volume fraction in $Sr_{1-x}Na_xFe_2As_2$, as a function of the sodium concentration.

Conclusions

In summary, we have reported on the synthesis, crystal and magnetic structures, and superconductivity transition temperatures for powder samples of the $Sr_{1-x}Na_xFe_2As_2$ solid solution in which compositions in the range $0 \leq x \leq 0.4$ are accessible in a single phase form using conventional solid state reactions as used for the other 122 members. Superconductivity appears for $x \geq 0.3$, and up to the phase limit, the low temperature structural transition driven by antiferromagnetic ordering coexists with superconductivity. The highest T_c of 26 K is found in $x = 0.4$ in which long-range magnetic order is still evident. At $x = 0.42$, phase separation starts to occur and Na-richer phases cannot be synthesized using high temperature methods.

Acknowledgment. We are grateful to Dr. R. I. Smith and Dr. M. F. Telling for assistance at ISIS and Dr. E. Suard for assistance at ILL. We acknowledge STFC for the provision of beamtime. Dr. R. Cortes-Gil acknowledges the support of a postdoctoral fellowship from *Ministerio de Educacion y Ciencia* of Spain.

Supporting Information Available: Lists of further refined structural parameters at ambient and low temperatures, diffractograms of samples just beyond the edge of the single phase region, and plots of the magnetic susceptibility for the sample with $x = 0.3$ (PDF). This material is available free of charge via the Internet at http://pubs.acs.org.